RSC Advances

COMMUNICATION

View Article Online
View Journal | View Issue

Cite this: *RSC Adv.*, 2015, **5**, 32369

Received 6th March 2015
Accepted 23rd March 2015

DOI: 10.1039/c5ra04028k

www.rsc.org/advances

New binuclear copper(II) coordination polymer based on mixed pyrazolic and oxalate ligands: structural characterization and mechanical properties†

Adaris M. López Marzo,‡[a] Miguel Guerrero,‡*[b] Teresa Calvet,[c] Mercè Font-Bardia,[d] Eva Pellicer,[b] Maria Dolors Baró,[b] Josefina Pons*[a] and Jordi Sort[e]

A new inorganic–organic coordination polymer based on a copper(II) binuclear complex coordinated with pyrazole (**L1**), 1-(hydroxymethyl)pyrazole) (**L2**) and oxalate (**Ox**) ligands has been unexpectedly obtained. The crystal structure of this coordination polymer has been unequivocally determined from single crystal X-ray diffraction. One copper(II) center (Cu1) is four-coordinated with two nitrogens (N2, L1 and N3, L2), one oxygen (O1, L1) and one chlorine atom, while the other copper(II) nucleus (Cu2) is five-coordinated with one nitrogen (N1, L1), three oxygens (O1, L2; O2 and O3, Ox) and one chlorine atom, giving slightly distorted square-planar and square-pyramidal geometries, respectively. To the best of our knowledge, such coordination environments have never been previously observed to coexist in the same structure. The terminal chlorine (Cl1) forms the connecting bridge between the planar binuclear $[Cu_2Cl(Ox)_{0.5}(L1)(L2)]_n$ units ending in an attractive structural framework. An extended layered structure staggered along the *b*-axis is observed in the supramolecular view. Nanoindentation experiments were carried out and relevant mechanical parameters such as hardness, Young's modulus, indentation energies and elastic recovery were determined. Additionally, a comparative analysis between the supramolecular structure and the mechanical properties is reported.

1. Introduction

The design of hybrid metal–organic materials (MOMs), which is a burgeoning topic in the crystal engineering domain, is nowadays one of the fastest growing areas in the fields of Materials Science and Supramolecular Chemistry.[1,2] This new class of materials attracts significant attention due to their enormous chemical, structural and topological diversity and due to their promising applications, including catalysis, gas storage, magnetism, luminescence, drug delivery, sensing or host/guest inclusion.[3–6] Interestingly, such hybrid systems present strong covalent and/or intermolecular bonds to yield 1D chains, 2D layers or 3D frameworks, which incorporate 3d-metal ions and bridging ligands at the same time. The synergy between the organic and inorganic components brings about an outstanding combination of properties that are not common in purely inorganic and organic systems alone. Furthermore, the use of different ligands with similar coordination abilities but different flexibilities as building blocks could be considered as a smart procedure for obtaining periodic frameworks.[7–9]

In contrast to the large number of recent publications describing the synthesis and characterization of MOM structures, studies focusing on understanding the mechanical properties of these hybrid materials are still scarce due to the lack of proper measurement tools.[10] Nonetheless, recent advances in this field are shedding some light on the fundamental structure–mechanical property relationships, which are needed for optimized design and successful performance in diverse technological applications.[11] Nanoindentation has emerged as a widely adopted technique for measuring the mechanical properties of different kinds of materials, such as ceramics, organics, inorganics and MOMs at the nanoscale level.[12] This technique, where load (P) and penetration depth (h) are measured at high resolution, enables not only the evaluation of the mechanical properties but also the correlation between the measured responses and the underlying structural features and intermolecular interactions.[13] This makes

[a]*Departament de Química, Universitat Autònoma de Barcelona, E-08193 Bellaterra, Spain*

[b]*Departament de Física, Universitat Autònoma de Barcelona, E-08193 Bellaterra, Spain. E-mail: Miguel.Guerrero@uab.cat; Tel: +34 93 581 1401*

[c]*Cristal lografia, Mineralogia i Dipòsits Minerals, Universitat de Barcelona, 08028-Barcelona, Spain*

[d]*Unitat de Difracció de RX, Centres Científics i Tecnològics de la Universitat de Barcelona (CCiTUB), Universitat de Barcelona, 08028-Barcelona, Spain*

[e]*Institució Catalana de Recerca i Estudis Avançats (ICREA), Departament de Física, Universitat Autònoma de Barcelona, E-08193 Bellaterra, Spain*

† Electronic supplementary information (ESI) available: X-ray crystallographic file in CIF format for the structure determination of the polymeric Cu(II) complex is enclosed. CCDC 1036962. For ESI and crystallographic data in CIF or other electronic format see DOI: 10.1039/c5ra04028k

‡ These authors have contributed equally to this work.

nanoindentation a complementary technique to structural analysis for the development of novel smart materials. In general, MOMs have been reported to be mechanically harder than inorganic polymers, while often exhibiting lower density values, similar to those of metallic foams.[14]

In this paper we present for the first time an inorganic–organic polymeric complex containing two different copper(II) *cores* with mixed oxalate ion and pyrazolic ligands. This new coordination polymer presents a 2D network along the *b*-axis formed by layers of stepped chains interconnected by bridging chlorine atoms (Cl1) through the Cu(1)–Cl(1)–Cu(2) bond. The hardness, Young's modulus, indentation energies and elastic recovery of this Cu(II) supramolecular inorganic/organic framework have been investigated by means of the nanoindentation technique and are compared with similar examples from the literature.

2. Experimental part

2.1 Reagents and synthesis

All reagents were purchased from Sigma-Aldrich and used as received without further purification. 1-(Hydroxymetyl)pyrazole (**L2**) was synthesized as described previously.[15]

In order to obtain the copper(II) based coordination complex, pyrazole (**L1**) and **L2** ligands were mixed with $CuCl_2 \cdot 2H_2O$ (1 : 1 : 2 molar ratio) for 18 h using ethanol as the solvent under aerobic conditions. The pH was adjusted to 9 with ammonium hydroxide solution (30% NH_3). The green powder obtained as the product was washed *via* vacuum filtration with a few milliliters of cold diethyl ether and dried at room temperature. Minority fraction and translucent blue prism-like monocrystals suitable for X-ray analysis were obtained through the crystallization of the synthesis product using an ethanol–dichloromethane (1 : 1) diffusion technique.

2.2 Characterization techniques

For X-ray crystallographic analysis, a translucent blue prism-like specimen of $C_8H_8ClCu_2N_4O_3$ ($M_w = 370.71$ g mol^{-1}), 0.145 mm × 0.252 mm × 0.290 mm, was used. X-ray intensity data were measured on a D8 Venture system equipped with a multilayer monochromator and a Mo microfocus ($\lambda = 0.71073$ Å). A total of 682 frames were collected. The total exposure time was 1.89 hours. The frames were integrated with the Bruker SAINT Software Package using a narrow-frame algorithm. The integration of the data using a monoclinic unit cell yielded a total of 13 166 reflections, to a maximum θ angle of 26.37° (0.80 Å resolution), out of which 2283 were independent (average redundancy 5767, completeness = 99.8%, $R_{int} = 3.44\%$, $R_{sig} = 2.24\%$) and 2121 (92.90%) were greater than $2\sigma(F^2)$. Elemental analysis (C, H, N) of the monocrystal-like specimen was carried out on a Carlo Erba CHNS EA-1108 instrument, separated by a chromatographic column and thermoconductivity detector. Copper elemental analysis was carried out using inductively coupled plasma mass spectrometry (ICPMS) with an Agilent 7500ce model system. Infrared (IR) spectra were recorded on a Perkin-Elmer FT spectrophotometer series 2000, in cm^{-1} and as KBr pellets. Conductivity measurements were performed at room temperature in 10^{-3} M methanol solutions, employing a CyberScan CON 500 (Eutech instrument) conductimeter. Electronic spectra were collected on a Kontron-Uvikon 860 in methanol, between 750 and 350 nm.

2.3 Mechanical properties

The mechanical properties (hardness, reduced elastic modulus and elastic recovery) were evaluated by means of nanoindentation, using a UMIS device from Fischer-Cripps Laboratories, equipped with a Berkovich pyramidal-shaped diamond tip, operating in the load control mode. The nanoindentation tests were performed perpendicular to the planar base (100) of the crystal sheet. Other orientations were not possible due to the crystal exfoliation of the material. Indentations using maximum applied load values ranging from 1 to 5 mN were applied to ensure that the maximum penetration depth was much smaller than the crystal thickness. The indentations were separated from each other by 20 μm, to ensure that the stress fields underneath the indents did not overlap with each other. The thermal drift during nanoindentation was lower than 0.05 nm s^{-1}. Proper corrections for the contact area (calibrated with a fused quartz specimen), instrument compliance, and initial penetration depth (a pre-contact load of 0.02 mN was used) were applied. The hardness (H) and reduced elastic modulus (E_r) values were derived from the load–displacement curves using the method of Oliver and Pharr.[16] From the initial unloading slope, the contact stiffness, S, was determined as:

$$S = \frac{dP}{dh} \quad (1)$$

The reduced Young's modulus was evaluated based on its relationship with the contact area, A, and S:

$$S = \beta \frac{2}{\sqrt{\pi}} E_r \sqrt{A} \quad (2)$$

where β is the King's factor, which depends on the geometry of the indenter ($\beta = 1.034$ for a Berkovich indenter).[17] The reduced Young's modulus takes into account the elastic displacements that occur in both the specimen, with Young's modulus E and Poisson's ratio ν, and the diamond indenter, with elastic constants E_i and ν_i (for diamond, $E_i = 1140$ GPa and $\nu_i = 0.07$):

$$\frac{1}{E_r} = \frac{1 - \nu^2}{E} + \frac{1 - \nu_i^2}{E_i} \quad (3)$$

The hardness was calculated from the following expression:

$$H = \frac{P_{max}}{A} \quad (4)$$

where P_{max} is the maximum load applied during nanoindentation. Finally, the elastic recovery was evaluated as the ratio between the elastic and the total (plastic + elastic) energies during nanoindentation, W_{el}/W_{tot}. The values of W_{el} were calculated as the area between the unloading curve and the displacement axis. In turn, W_{tot} is the area between the loading

curve and the displacement axis.[18] The results presented in this work are the statistical average of a set of 10 indentations at the applied maximum load.

3. Results and discussion

3.1 Crystal structure of the binuclear copper(II) based coordination polymer

The reaction of L1 and L2 ligands with $CuCl_2 \cdot 2H_2O$ (1 : 1 : 2 molar ratio) was carried out in ethanol. The recrystallization of the reaction product afforded minority fraction blue prism-like monocrystals. The X-ray diffraction measurements performed on the obtained monocrystals revealed that the complex crystallizes in the $P2(1)/c$ space group with two independent Cu(II) metal centers having square-planar and square-pyramidal geometries, respectively (Fig. 1). The complex presents a polymeric structure showing a one-dimensional (1D) infinite neutral chain of planar binuclear $[Cu_2Cl(Ox)_{0.5}(L1)(L2)]_n$ units, wherein both L1–L2 ligand bridges are adjacent the different copper(II) centers. Additional characterization of these monocrystals was carried out.[19]

The local coordination environment around the four-coordinated Cu(II) atom (Cu1) is formed by two pyrazolyl (pz) nitrogen atoms (N2 and N3 in L1 and L2 ligands, respectively), one alcohol oxygen atom (O1, L2) and one bridged chlorine atom (Cl1). The coordination sphere of Cu1 can be described as a slightly distorted square-planar geometry with N2–Cu1–O1 and N3–Cu1–Cl1 angles between 81.17(7)° and 94.26(5)°, respectively, which is within the expected range for copper(II) compounds with a square-planar geometry. The Cu1–O1, Cu1–N2 and Cu1–N3 bond distances have similar values in the 1.937–1.945 Å range, indicating a stronger coordination than the Cu1–Cl1 bond (2.25 Å). The $[CuClO(N_{pz})_2]$ *core* has been previously reported in the literature[20–23] but never as a building block of a polymeric structure. Selected values of bond lengths and bond angles for the complex as well as the corresponding crystallographic data are shown in Table 1 and Table 2, respectively.

Regarding the five-coordinated Cu2 atom, the basal plane is formed by one pyrazolyl nitrogen atom (N1, L1), one alcohol oxygen atom (O1, L2) and two chelated oxygen atoms from the oxalate anion (O2 and O3, Ox). These four coordinated atoms together with the Cu2 ion define an almost perfect planar arrangement. The Cu2 atom is slightly displaced 0.124(2) Å from the basal NO3 plane. The chlorine atom (Cl1) is

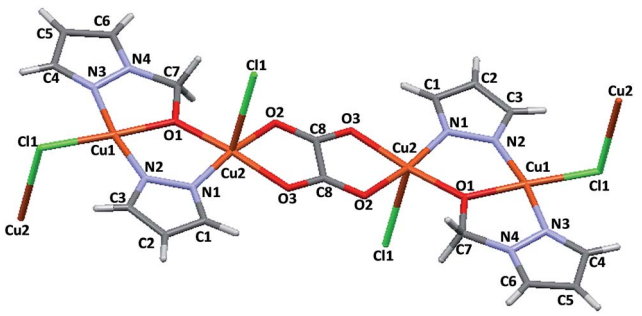

Fig. 1 X-Ray structure of the $[Cu_4Cl_2(Ox)(L1)_2(L2)_2]$ complex, where $[Cu_2Cl(Ox)_{0.5}(L1)(L2)]$ is the basic monomeric unit of this polymeric chain. Colour scheme: copper, orange; oxygen, red; chlorine, green; nitrogen, blue and carbon, grey.

Table 1 Selected bond lengths (Å) and bond angles (°) for the (a) square-planar and (b) square-pyramidal copper(II) geometries of the complex. Symmetry code: #1 $-x + 1, -y + 1, -z$

Geometries	Bond lengths (Å) and bond angles (°)	
a) 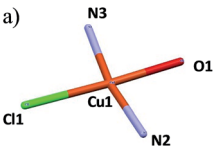	Cu(1)–N(2)	1.9371(17)
	Cu(1)–N(3)	1.9441(18)
	Cu(1)–O(1)	1.9448(14)
	Cu(1)–Cl(1)	2.2569(5)
	N(2)–Cu(1)–O(1)	89.18(7)
	N(3)–Cu(1)–O(1)	81.17(7)
	N(2)–Cu(1)–Cl(1)	95.45(5)
	N(3)–Cu(1)–Cl(1)	94.26(5)
b) 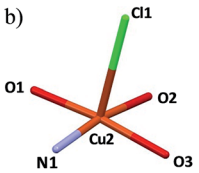	Cu(2)–N(1)	1.9257(17)
	Cu(2)–O(1)	1.9318(14)
	Cu(2)–O(2)	1.9679(14)
	Cu(2)–O(3)#1	1.9991(14)
	Cu(2)–Cl(1)	2.795(4)
	N(1)–Cu(2)–O(1)	89.00(7)
	O(2)–Cu(2)–O(1)	95.59(6)
	N(1)–Cu(2)–O(3)#1	89.92(7)
	O(2)–Cu(2)–O(3)#1	84.78(6)
	O(3)#1–Cu(2)–Cl(1)	92.57(5)

Table 2 Crystallographic data for the copper(II) complex

Molecular formula	$C_8H_8ClCu_2N_4O_3$
Formula weight	370.71
Temperature (K)	100 (2)
Wavelength (Å)	0.71073
System, space group	Monoclinic, $P2_1/c$
Unit cell dimensions	
a (Å)	10.5078(7)
b (Å)	9.1266(6)
c (Å)	11.7875(8)
α (°)	90
β (°)	99.869(3)
Γ (°)	90
U (Å^3)	1113.70(13)
Z	4
D_{calc} (mg m^{-3})	2.211
μ (mm^{-1})	4.062
F (000)	732
Crystal size (mm^3)	0.290 × 0.252 × 0.145
hkl ranges	$-13 \le h \le 13$
	$-11 \le k \le 11$
	$-14 \le l \le 14$
2θ range (°)	2.84 to 26.37
Reflections collected/unique/[R_{int}]	13166/2283 [R(int) = 0.0344]
Completeness to θ	99.8% (θ = 25.242°)
Absorption correction	Semi-empirical from equivalents
Data/restraints/parameters	2283/54/163
Goodness-of-fit on F^2	1.058
Final R indices [$I > 2\sigma(I)$]	R_1 = 0.0208, wR_2 = 0.0545
R indices (all data)	R_1 = 0.0232, wR_2 = 0.0559
Largest diff. peak and hole (e Å^{-3})	0.444 and −0.412

coordinated to the apical position of the Cu2 site with a longer bond distance of 2.795(3) Å. The coordination sphere of Cu2 can be described as a slightly distorted square-pyramidal geometry with O(2)–Cu(2)–O(1) and O(2)–Cu(2)–O(3) angles between 84.78(6) and 95.59(6)°, respectively, and Cu(2)–O(1), Cu(2)–O(2), Cu(2)–O(3) and Cu(2)–N(1) bond distances of 1.932, 1.968, 1.999 and 1.926 Å, respectively. Such angles and bond distances are within the expected range for copper(II) compounds with square-pyramidal geometry. In the crystal structure of the Cu2 metal centers with square-pyramidal geometry are connected to each other *via* one oxalate anion (Ox) ligand through a bis-bidentate chelating mode, with adjacent Cu(II) atoms at 5.164 Å (μ-oxalato-1κ^{2}O^1,O^2:2κO^{1a},O^{2a}). The Cu–Ox distances fall within the typical range for oxalate bridged Cu(II) complexes.[24–26] The Cu1···Cu2 distance of 3.350 Å is out of the limit of the interactive range between the different copper atoms (van der Waals radius of Cu(II) is 2.8 Å). The pyrazole rings are nearly parallel with a dihedral angle of 3.15(1)° between their planes.

The unexpected formation of the oxalate anion in the reaction medium could be attributed to the ethanol oxidation by dissolved O_2, favored by the basicity of the medium and the catalytic properties of the copper(II) ions (the reaction took place under aerobic and basic conditions). Copper(II) ions could cause the catalytic activation of O_2 and OH^- to produce reactive species (*i.e.* hydroxyl radicals, $OH^{\bullet -}$) capable of oxidizing a minor fraction of the ethanol solvent. Using the spectrophotometric method, traces of oxalic acid were found after stirring a basic solution of ethanol and $CuCl_2$ under aerobic conditions.[27] Similar oxalate occurrence was reported by Jing Su *et al.*[28] and Mansour Arab *et al.*[29] The possible reactions involved in the synthesis process of the complex presented here are illustrated in Scheme 1.

The "*in situ*" formation of oxalic acid from solvent during the complex formation reaction has been previously reported.[30,31] In addition, there are also previous reports of aerobic alcohol oxidation during the formation of copper coordination complexes or in the presence of copper salts.[32–34] In all these cases the alcohol oxidation is related to the catalytic properties of copper(II) ions.

Copper, with a dynamic Jahn–Teller distortion,[35] efficiently catalyzes the oxidation of organic compounds under mild conditions and can provide open Lewis acid sites which are effective for catalysing various organic reactions, such as azide–alkyne cycloaddition, oxidative coupling reactions, Henry or Diels–Alder reactions,[36–38] or water oxidation,[39] among others.

This binuclear copper(II) based coordination polymer owes its particularity to the fact that it is composed of three different ligands, where neither of the [$CuClO_3N_{pz}$] and [N_{pz}–Cu–Ox–Cu–N_{pz}] coordination environments have been reported before.[40] Only the [$CuClO(N_{pz})_2$] *core* presents a similar coordination sphere to that already described.[20–23,] Such special coordination spheres provide interesting structures in the network of this complex.

In the supramolecular crystal arrangement, each [Cu_4Cl_2(Ox)(L1)$_2$(L2)$_2$] molecule is surrounded by 4 other neighbouring molecules in the unit cell. The disposition of these molecules in the unit cell is a typical ABAB structure. Zig-zag layers of polymeric chains interconnected by chloride bridges between the intermolecular copper centers afford a 2D structure along the *b* axis in the supramolecular framework (Fig. 2A). The chlorine atoms (Cl1) are the bridges between one molecule and the other through the Cu2–Cl1–Cu1 bond with a 93.02° angle. In addition, the intramolecular contacts between the N3···Cl1···N2 atoms (3.086 and 3.111 Å, respectively) contribute to support the supramolecular network (Fig. 2B). The staggered layered structure determines the mechanical properties measured for this polymer using the nanoindentation technique.

3.2 Mechanical properties of the binuclear copper(II) based coordination polymer

Representative nanoindentation curves, performed perpendicular to the planar base of the crystal, that corresponds to the (100) face, and up to maximum loads of 1.2 and 2.8 mN, are shown in Fig. 3a and S1.† Measurement of the mechanical properties by nanoindentacion along the other directions was not possible because of the high tendency for the crystals

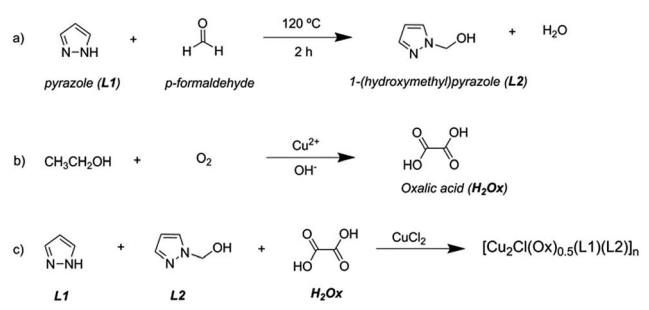

Scheme 1 Chemical reactions involved in obtaining the polymeric complex: synthesis of the L2 ligand (a), *in situ* formation of oxalic acid (b) and complex formation (c).

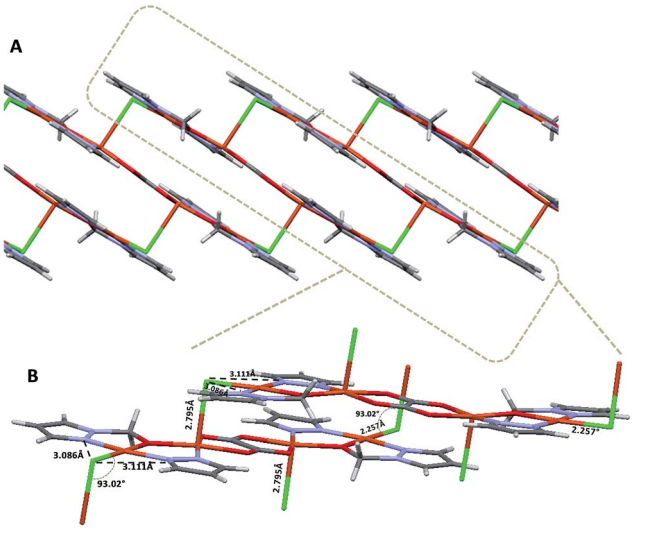

Fig. 2 (A) Polymeric layer structure with zig-zag distribution along the *b* axis. (B) The close-up view displays the distances and the angles formed by the Cu1–Cl1–Cu2 intermolecular bridges.

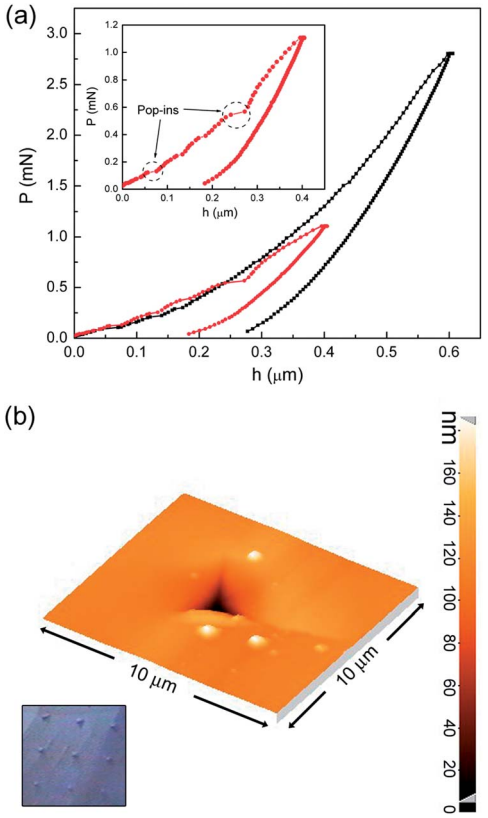

Fig. 3 (a) Representative nanoindentation curves performed perpendicular to the crystal sheet, and up to maximum loads of 1.2 mN (red line) and 2.8 mN (black line). (b) Atomic force microscopy and optical (inset) images of an indentation performed using a maximum load of 2.8 mN.

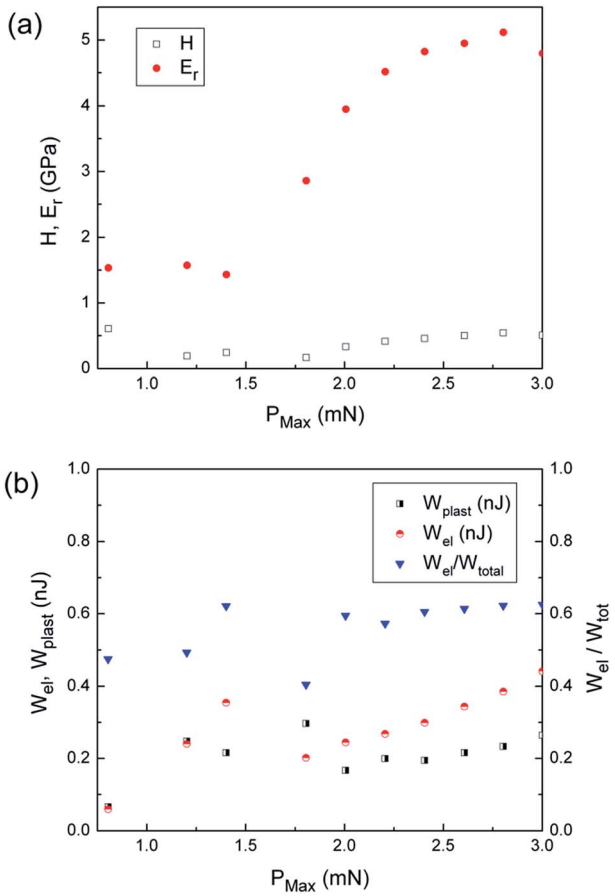

Fig. 4 Values of (a) hardness and reduced Young's modulus and (b) indentation energies and elastic recovery (W_{el}/W_{tot}) of the complex.

towards brittle fracture. Discontinuities or pop-in events in the loading segments are often observed and are ascribed to the breakage of molecular stacks and the concomitant sudden penetration of the indenter deeper into the sample.

The atomic force microscopy image (Fig. 3b) of an indentation performed using a maximum load of 2.8 mN shows that pile-up effects are virtually absent, while crack formation from the edge of the triangular imprint sometimes occurs, an observation which is in agreement with the occurrence of serrations in the loading segments of the indentation curves (Fig. 3a). The lack of pile-up avoids artifacts related to the determination of the contact area from the contact depth, when using the method of Oliver and Pharr.[16]

The values of hardness, reduced Young's modulus, indentation energies and elastic recovery (W_{el}/W_{tot}) are shown in Fig. 4a and b. Hardness remains rather constant ($H \approx 0.4$–0.5 GPa) as a function of the applied maximum load (Fig. 4a). This value is a bit higher than the ones reported by C. M. Reddy *et al.*[41] for 2-(methylthio)nicotinic acid and similar to values reported by J. C. Tan *et al.* for different low-symmetry polymorphs of copper phosphonoacetates $[Cu_{1.5}(H_2O)(O_3PCH_2CO_2)]$.[42] Conversely, the Young's modulus is a bit lower than the values reported for some other molecular crystals[13,42,43] but similar to the values reported by A. Samanta *et al.* for $[OZn_4(BDC)_3]_n$, where BDC stands for 1,4-benzenedicarboxylate anion.[44] The increase of E_r with the applied load indicates a higher resistance against elastic deformation as the penetration depth is progressively increased. This could be due to the larger amount of molecular bonds which hinder the elastic deformation as the applied load is progressively increased. Nevertheless, no clear changes in the elastic energy or the elastic recovery are observed in the range of applied loads used in this study (Fig. 4b). The value of elastic recovery ($W_{el}/W_{tot} \approx 0.6$) is clearly larger than those of other types of organic–inorganic materials[45] and is comparable to the values in some recent reports on 3D inorganic composite films.[46]

4. Conclusions

A new binuclear copper(II) complex with a polymeric structure has been unexpectedly obtained from a mixture of pyrazolic ligands and $CuCl_2$ in ethanol. The two copper(II) centers have different coordination numbers and geometries. The Cu1 atom is four-coordinated in the $[CuClO(N_{pz})_2]$ *core* with a square-planar molecular geometry, while the Cu2 nucleus is five-coordinated with $[CuClO_3N_{pz}]$ *core* and exhibits square-pyramidal geometry. Furthermore, the Cu2 centers of different molecular units are interconnected in the polymeric

structure *via* one unexpected oxalate anion. The terminal chlorine atoms act as bridges between the monomeric units in this coordination polymer. As far as we know, this is the first time that the $[CuClO_3N_{pz}]$ and $[N_{pz}–Cu–Ox–Cu–N_{pz}]$ coordination environments are reported. In the supramolecular network an interesting 2D structure with layered architecture formed from polymeric chains interconnected by Cu2–Cl1–Cu1 bridges is formed along the *b*-axis. Additionally, the values of hardness, Young's modulus, and elastic recovery of this structure have been determined by means of nanoindentation. The mechanical characterization of this kind of hybrid material is an important asset to crystal engineering since durability and reliability, which are dictated by the mechanical properties, are important factors for their potential applications in sensors, catalysts and gas storage, among others.

Acknowledgements

The financial support from the MAT2011-27380-C02-01 and the MAT2011-27225 research projects from the Spanish MINECO, and the 2014-SGR-1015 and the 2014-SGR-260 projects from the Generalitat de Catalunya are acknowledged. M. D. B. was partially supported by an ICREA-Academia award. A. L_M. thanks the FI-2010 scholarship given by the Government of Catalonia. M. G. acknowledges the support of the Secretary for Universities and Research of the Government of Catalonia and the COFUND Programme of the Marie Curie Actions of the 7th R & D Framework Programme of the European Union for the 'Beatriu de Pinos' contract (2013 BP-B 00077). E. P. acknowledges the Spanish MINECO for the 'Ramon y Cajal' contract (RYC-2012-10839).

References

1 T. R. Cook, Y.-R. Zheng and P. J. Stang, *Chem. Rev.*, 2013, **113**, 734–777.
2 M. Eddaoudi, J. Kim, N. Rosi, D. Vodak, J. Wachter, M. O'Keeffe and O. M. Yaghi, *Science*, 2002, **295**, 469–472.
3 I.-H. Park, A. Chanthapally, Z. Zhang, S. S. Lee, M. J. Zaworotko and J. J. Vittal, *Angew. Chem., Int. Ed.*, 2014, **53**, 414–419.
4 S. Xiang, Y. He, Z. Zhang, H. Wu, W. Zhou, R. Krishna and B. Chen, *Nat. Commun*, 2012, **3**, 954–963.
5 X.-L. Yang, M.-H. Xie, C. Zou, Y. He, B. Chen, M. O'Keeffe and C.-D. Wu, *J. Am. Chem. Soc.*, 2012, **134**, 10638–10645.
6 Y. Zhao, D.-S. Deng, L.-F. Ma, B.-M. Ji and L.-Y. Wang, *Chem. Commun.*, 2013, **49**, 10299–10301.
7 L. Croitor, E. B. Coropceanu, D. Chisca, S. G. Baca, J. van Leusen, P. Kögerler, P. Bourosh, V. C. Kravtsov, D. Grabco, C. Pyrtsac and M. S. Fonari, *Cryst. Growth Des.*, 2014, **14**, 3015–3025.
8 L. J. McCormick, S. G. Duyker, A. W. Thornton, C. S. Hawes, M. R. Hill, V. K. Peterson, S. R. Batten and D. R. Turner, *Chem. Mater.*, 2014, **26**, 4640–4646.
9 F. Gul-E-Noor, M. Mendt, D. Michel, A. Pöppl, H. Krautscheid, J. Haase and M. Bertmer, *J. Phys. Chem. C*, 2013, **117**, 7703–7712.
10 J. C. Tan and A. K. Cheetham, *Chem. Soc. Rev.*, 2011, **40**, 1059–1080.
11 W. Li, M. S. R. N. Kiran, J. L. Manson, J. A. Schlueter, A. Thirumurugan, U. Ramamurty and A. K. Cheetham, *Chem. Commun.*, 2013, **49**, 4471–4473.
12 S. Varughese, M. S. R. N. Kiran, U. Ramamurty and G. R. Desiraju, *Angew. Chem., Int. Ed.*, 2013, **52**, 2701–2712.
13 J. C. Tan, J. D. Furman and A. K. Cheetham, *J. Am. Chem. Soc.*, 2009, **131**, 14252–14254.
14 S. S. Han and W. A. Goddard, *J. Phys. Chem. C*, 2007, **111**, 15185–15191.
15 W. L. Driessen, *Recl. Trav. Chim. Pays-Bas*, 1982, **101**, 441–443.
16 W. C. Oliver and G. M. Pharr, *J. Mater. Res.*, 1992, **7**, 1564–1583.
17 A. Fischer-Cripps, *Nanoindentation*, Springer, New York, USA, 2004.
18 E. Pellicer, A. Varea, S. Pané, B. J. Nelson, E. Menéndez, M. Estrader, S. Suriñach, M. D. Baró, J. Nogués and J. Sort, *Adv. Funct. Mater.*, 2010, **20**, 983–991.
19 Analysis for $C_8H_8ClCu_2N_4O_3$ calcd/found (%): C, 25.92/25.72; H, 2.17/2.13, N, 15.11/15.04, Cu, 34.28/33.96, giving satisfactory C, H, N and Cu elemental analyses. IR (KBr, cm^{-1}): 3190, 3120 $\nu(C–H)_{ar}$; 2940, 2920 $\nu(C–H)_{al}$; 1650 $[\nu(C{=}C), \nu(C{=}N)]_{ar}$; 1400 $[\delta(C{=}C), \delta(C{=}N)]_{ar}$ and 773 $\gamma(=C–H)_{oop}$ present shifts (in relation with the free ligand) produced by the coordination with copper(II); moreover, the bands at 472, 428 ν(Cu–N); 550, ν(Cu–O); 600 γ_{as}(Cu–O) and 356, 322 ν(Cu–Cl) also corroborate the copper coordination. Conductivity (1.02×10^{-3} M in methanol): 32 Ω^{-1} cm^2 mol^{-1}, in agreement with a non-electrolyte complex; UV-vis (1.1×10^{-3} M in methanol) exhibits a single band at 620 nm.
20 G. Mezei, M. Rivera-Carrillo and R. G. Raptis, *Inorg. Chim. Acta*, 2004, **357**, 3721–3732.
21 G. Mezei, R. G. Raptis and J. Telser, *Inorg. Chem.*, 2006, **45**, 8841–8843.
22 M. Rivera-Carrillo, I. Chakraborty, G. Mezei, R. D. Webster and R. G. Raptis, *Inorg. Chem.*, 2008, **47**, 7644–7650.
23 P. A. Angaridis, P. Baran, R. Boca, F. Cervantes-Lee, W. Haase, G. Mezei, R. G. Raptis and R. Werner, *Inorg. Chem.*, 2002, **41**, 2219–2228.
24 M. F. Castello, C. V. Grupioni, R. S. Nunes and J. M. Luiz, *J. Therm. Anal. Calorim.*, 2014, **117**, 1145–1150.
25 X.-D. Zhang, Z. Zhao, J.-Y. Sun, Y.-Ch. Ma and M.-L. Zhu, *Acta Crystallogr., Sect. E: Struct. Rep. Online*, 2005, **61**, m2643–m2645.
26 H.-D. Wang, Y.-L. Zhou, H.-Y. He, X.-H. Tu and L.-G. Zhu, *Acta Crystallogr., Sect. E: Struct. Rep. Online*, 2006, **62**, m1081–m1082.
27 Traces of oxalic acid were determined by a spectrophotometric method under aerobic conditions after stirring a basic solution of $CuCl_2$ in ethanol. The oxalic acid concentration was determined from the decrease in absorbance of the Cu^{2+} band and the increase of the Cu–Ox one, changing the colour from blue to yellow.

28 J. Su, Y.-Q. Sun, F.-J. Huo, Y.-T. Yang and C.-X. Yin, *Analyst*, 2010, **135**, 2918–2923.
29 M. Arab Chamjangali, L. Sharif-Razavian, M. Yousefi and A. Hossein Amin, *Spectrochim. Acta, Part A*, 2009, **73**, 112–116.
30 O. R. Evans and W. Lin, *Cryst. Growth Des.*, 2001, **1**, 9–11.
31 C. S. Hawes and P. E. Kruger, *Aust. J. Chem.*, 2013, **66**, 401–408.
32 I. Gamba, I. Mutikainen, E. Bouwman, J. Reedijk and S. Bonnet, *Eur. J. Inorg. Chem.*, 2013, 115–123.
33 N. Mase, T. Mizumori and Y. Tatemoto, *Chem. Commun.*, 2011, **47**, 2086–2088.
34 R. A. Sheldon, *Catal. Today*, 2015, **247**, 4–13.
35 M. A. Halcrow, *Chem. Soc. Rev.*, 2013, **42**, 1784–1795.
36 J. Park, J.-R. Li, Y.-P. Chen, J. Yu, A. A. Yakovenko, Z. U. Wang, L.-B. Sun, P. B. Balbuena and H.-C. Zhou, *Chem. Commun.*, 2012, **48**, 9995–9997.
37 I. H. Hwang, J. M. Bae, W.-S. Kim, Y. D. Jo, C. Kim, Y. Kim, S.-J. Kim and S. Huh, *Dalton Trans.*, 2012, **41**, 12759–12765.
38 Y. Zhao, D.-S. Deng, L.-F. Ma, B.-M. Ji and L.-Y. Wang, *Chem. Commun.*, 2013, **49**, 10299–10301.
39 T. Zhang, C. Wang, S. Liu, J.-L. Wang and W. Lin, *J. Am. Chem. Soc.*, 2014, **136**, 273–281.
40 ESI.†
41 C. M. Reddy, R. C. Gundakaram, S. Basavoju, M. T. Kirchner, K. A. Padmanabhan and G. R. Desiraju, *Chem. Commun.*, 2005, 3945–3947.
42 J. C. Tan, C. A. Merrill, J. B. Orton and A. K. Cheetham, *Acta Mater.*, 2009, **57**, 3481–3496.
43 C. Malla, G. Reddy, R. Krishnaa and S. Ghosha, *CrystEngComm*, 2010, **12**, 2296–2314.
44 A. Samanta, T. Furuta and J. Li, *J. Chem. Phys.*, 2006, **125**, 084714.
45 C. Schütz, J. Sort, Z. Bacsik, V. Oliynyk, E. Pellicer, A. Fall, L. Wågberg, L. Berglund, L. Bergström and G. Salazar-Álvarez, *PLoS One*, 2012, **7**, e45828.
46 M. Guerrero, S. Pané, B. J. Nelson, M. D. Baró, M. Roldán, J. Sort and E. Pellicer, *Nanoscale*, 2013, **5**, 12542–12550.